Progress In Electromagnetics Research M, Vol. 44, 69–79, 2015

Low-Loss Complex Permittivity and Permeability Determination in Transmission/Reflection Measurements with Time-Domain Smoothing

Sung Kim* **and Jeffrey R. Guerrieri**

Abstract—An approach is proposed for determination of the complex permittivity and permeability of low-loss materials, eliminating half-wavelength resonances occurring in transmission/reflection (T/R) measurements. To this end, we apply time-domain smoothing for removing resonant artifacts from the wave impedance obtained with the conventional T/R method, assuming that we do not have such artifacts in the refractive index. Accordingly, the permittivity and permeability are found from the smoothed wave impedance and conventional refractive index. Our method is validated by measurements for two different low-loss materials, nylon and lithium ferrite, and those results are discussed. Further, results from the present approach are compared to those from the approximate approach derived in our previous work.

1. INTRODUCTION

Electromagnetic characterizations of materials have been long carried out to support fundamental engineering research and development (R&D) and application product design activities. The precise knowledge of material properties is of great importance to make effective use of the characterizations of materials. To date, various measurement techniques for the characterizations have been suggested, and computational algorithms for determining material parameters that suit each of those measurement techniques have been derived [1–4].

The conventional transmission/reflection (T/R) method [5–10] has been known as one of the broadband techniques that extract complex permittivity and permeability from total transmission and reflection coefficients measured for a sample-loaded transmission line, i.e., coaxial line, rectangular waveguide, etc., at microwave frequencies. The T/R method has often proved useful to measure well-machined solid material samples over a broad range of frequency.

Although the conventional T/R method is often well-suited for broadband measurements to characterize materials, there remain inherent issues to be resolved. In our previous study [11], we circumstantially investigated one of those issues that arise in the T/R method — artifacts that arise in the material parameters extracted near half-wavelength ($\lambda/2$) resonances when measuring a low-loss material with the conventional T/R method. These artifacts stem from geometric resonances called Fabry-Pérot resonances (FPRs) that appear when a test sample has a low-loss material property and its dimension is an integer multiple of $\lambda/2$ [12–14]. The resonances are, in effect, standing waves created by multiple reflections that occur between air-to-sample and sample-to-air interfaces in the transmission line and are due to the discontinuity of the material property of the air and sample. The resonant artifacts can severely reduce accuracy in permittivity and permeability measurements with the conventional T/R method.

Received 30 July 2015, Accepted 29 September 2015, Scheduled 13 October 2015

* Corresponding author: Sung Kim (sung.x.kim@nist.gov).

The authors are with the Radio Frequency Technology Division, Communications Technology Laboratory, National Institute of Standards and Technology, 325 Broadway, Boulder, CO 80305, USA.

In [11], we approximated the input impedance of the sample-loaded transmission line by means of 1st-order regressions to remove resonant artifacts. From this approximate input impedance, we calculated the characteristic impedance of the sample-filled section that is, in turn, either a function of the wave impedance of the material filling a coaxial line or a function of the permeability filling a rectangular waveguide. Using the wave impedance or the permeability calculated from the characteristic impedance, the permittivity was computed, supplemented with the refractive index found by the conventional T/R method. In this way, the approximate approach in [11] was able to provide reasonable estimates of the material parameters near the frequencies associated with geometric resonances in T/R measurements made on low-loss materials.

This present work, which is an alternative to the technique introduced in [11], proposes a more accurate approach to determining the complex permittivity and permeability of low-loss materials for frequencies near geometric resonances or (FPRs). Similar to [11], this new approach starts with an assumption that the T/R method ensures a smooth refractive index at all frequencies, but in contrast employs the inverse discrete Fourier transform (DFT) of a frequency response for the wave impedance that is obtained from the conventional T/R method, with an appropriately truncated frequency range. Subsequently, in this time-domain regime, we use windowing to permit zero-time components of the wave impedance. To obtain the smoothed wave impedance as a function of frequency, we then apply the forward DFT to this modified time-domain wave impedance. Thereafter, the permittivity and permeability are calculated from this smoothed wave impedance and the conventional refractive index. We then validate the present method by measurements on nylon and lithium ferrite samples with an APC-7 coaxial transmission line, comparing these results to those in [11].

2. COMPUTATIONAL METHOD

2.1. Theoretical Background of the T/R Method

The T/R method employs a frequency response of S-parameters measured for a test material sample slab placed in a transmission line (coaxial line, rectangular waveguide, etc.), as illustrated in Fig. 1. In Fig. 1, an electromagnetic wave is incident upon the surface of the sample of length L and is reflected and transmitted, respectively, from the front and back surface.

The reflection and transmission parameters, S_{11} and S_{21}, as measured at reference planes 1 and 2 (or S_{22} and S_{12} at reference planes 2 and 1), are given by

$$S_{11} = S_{22} = \frac{\Gamma\left(1 - P^2\right)}{1 - \Gamma^2 P^2}, \tag{1}$$

$$S_{21} = S_{12} = \frac{P\left(1 - \Gamma^2\right)}{1 - \Gamma^2 P^2}, \tag{2}$$

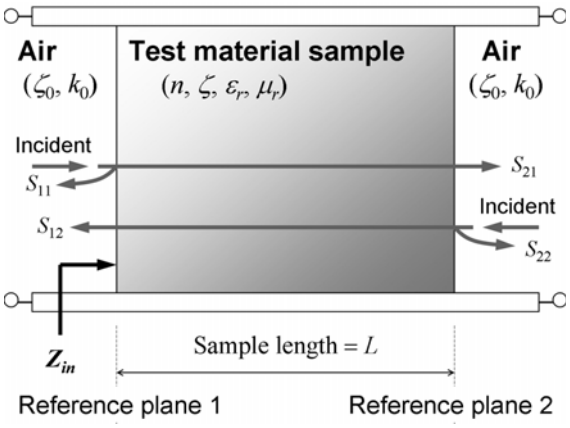

Figure 1. Schematic illustration of the S-parameters measured for the test material sample slab placed in a transmission line.

where Γ is the reflection coefficient of the interface, and P is the phase factor that represents the phase shift of the wave traveling through the material slab. Because in this paper we use an APC-7 coaxial line as a sample fixture that supports transverse electromagnetic (TEM) propagation waves, Γ and P are expressed as

$$\Gamma = \frac{\varsigma - \varsigma_0}{\varsigma + \varsigma_0}, \tag{3}$$

$$P = \exp\left(-j\frac{2\pi nL}{\lambda_0}\right), \tag{4}$$

where ς is the wave impedance of the test material, $\varsigma_0 (\cong 377\,\Omega)$ is the wave impedance of air, j is $\sqrt{-1}$, λ_0 is the wavelength in air, and n is the refractive index of the material.

In order to extract the material parameters n and ς from the S-parameters measured for the material slab, we need to simultaneously solve Eqs. (1) and (2) (we usually need to measure only either a pair of S_{11} and S_{21} or a pair of S_{22} and S_{12}). In practice, these equations can be solved in an explicit or iterative manner. The former is known as the Nicolson-Ross-Weir (NRW) method [5, 6] while the latter is often referred to as the Baker-Jarvis (BJ) iteration method [8, 9]. Eqs. (1) and (2) can be further reformulated for the BJ iteration method, resulting in the reference-plane invariant method occasionally called the NIST precision method (see [8, 9]).

The non-iterative explicit technique in the TEM case conveniently allows us to get simple analytical solutions [11]:

$$X = \frac{\left(S_{11}^2 - S_{21}^2\right) + 1}{2S_{11}}, \tag{5}$$

$$\Gamma = X \pm \sqrt{X^2 - 1}, \tag{6}$$

$$P = \frac{(S_{11} + S_{21}) - \Gamma}{1 - (S_{11} + S_{21})\,\Gamma}, \tag{7}$$

$$n = n' - jn'' = \pm j\frac{\lambda_0}{2\pi L}\ln\left(\frac{1}{P}\right) = \pm j\frac{\lambda_0}{2\pi L}\left[\ln\left(\frac{1}{P}\right) + j2\pi m\right], \tag{8}$$

$$\varsigma_r = \frac{\varsigma}{\varsigma_0} = \varsigma_r' + j\varsigma_r'' = \pm\sqrt{\frac{(1+S_{11})^2 - S_{21}^2}{(1-S_{11})^2 - S_{21}^2}}. \tag{9}$$

The ln symbol on the right-hand side of Eq. (8) denotes the principal value of the natural logarithm. Since the material is passive, $+/-$ signs in Eqs. (6), (8) and (9) should be chosen to satisfy physical constraints, $|\Gamma| \leq 1$, $n'' \geq 0$ and $\varsigma' \geq 0$, respectively. Note that n' can be negative when measuring 'effective' parameters of a negative-index medium [15–18]. If the material does not possess a very dispersive characteristic, we can readily find a correct value of the integer m in Eq. (8) in such a way that the group delay acquired from the value of n calculated from Eq. (8) matches the one obtained from the measurement [6].

Further, we can determine the relative values of the complex dielectric permittivity ε_r and magnetic permeability μ_r from n and ς_r as follows:

$$\varepsilon_r = \varepsilon_r' - j\varepsilon_r'' = n/\varsigma_r, \tag{10}$$

$$\mu_r = \mu_r' - j\mu_r'' = n \cdot \varsigma_r. \tag{11}$$

2.2. The Issue for the T/R Method

In [11], we extensively studied an unavoidable issue that inherently occurs in measurements for low-loss materials with the conventional T/R method, which we briefly review here.

One of the well known issues for the T/R method is that when measuring a low-loss material, resonant artifacts arise in the permittivity and permeability extracted near frequencies where the sample length L corresponds to an integer multiple of a half wavelength ($\lambda/2$). This issue is attributed to geometric resonances or FPRs occurring within the low-loss material sample of length of $L = \lambda/2$ due to the discontinuity of the material property of the air and sample in the transmission line. In [11], this

physical phenomenon was in detail explained and confirmed by the fact that, looking from reference plane 1 in Fig. 1, the input impedance Z_{in} of the sample-loaded section of the transmission line appears to be nearly equal to the characteristic impedance of the air section, $Z_0(= 50\,\Omega$ for an APC-7 coaxial line), at the resonant frequencies. Thus, at the resonant frequencies, $|S_{11}|$ and $|S_{21}|$ have, respectively, negative (minimal) and positive (maximal) peaks, i.e., $|S_{11}| \cong 0$ and $|S_{21}| \cong 1$ for a significantly low-loss material. It can also be understood that those resonances are created by dominant-mode standing waves reflected back and forth within the test sample (if the resonances were due to higher-order modes, $|S_{21}|$ would be small because those modes are evanescent and do not propagate). As was done in [11], in this paper we assume that the sample is homogeneous and appropriately machined, and has sufficiently flat and smooth front and back surfaces, so that only a dominant mode can exist in the sample-loaded transmission line. If a composite material sample is measured and resonances that arise from higher-order evanescent waves need to be taken care of, see the literature [19, 20].

Equation (9) provides a fairly intuitive explanation about the issue in the extraction of material parameters with the conventional T/R method. We can see from Eq. (9) that ς_r becomes ill-conditioned when $|S_{11}| \cong 0$ and $|S_{21}| \cong 1$. As a result, the wave impedance ς_r gets significantly divergent at the $\lambda/2$ frequencies. As was discovered in [11, 21], in general, the refractive index n obtained from Eq. (8) is sufficiently smooth over the entire frequency range, whereas the wave impedance ς_r has very strong resonances appearing as sharp peaks at the $\lambda/2$ frequencies. Such n and ς_r give rise to artifacts in the dielectric permittivity ε_r and magnetic permeability μ_r derived from Eq. (10) and (11) at those frequencies. In real-life measurements, any vector network analyzers (VNAs) that have finite dynamic range cannot accurately measure very small S-parameters, $|S_{11}| \cong 0$, and this measurement limitation is another source of degradation of measurements at the $\lambda/2$ frequencies.

2.3. Smoothing in the Time Domain

Figure 2 depicts a conceptual drawing for a frequency response of the wave impedance ς_r of a low-loss material measured with the T/R method around a $\lambda/2$ frequency. Fig. 2 illustrates that, as has been discussed in Subsection 2.2, the wave impedance obtained from the T/R method is divergent and appears to be resonant at the $\lambda/2$ frequency, whether we use the explicit or iterative technique to solve Eqs. (1) and (2).

In order to circumvent the issue of the resonant artifacts in the material parameters extracted with the T/R method, we attempt to get rid of the resonant peak in the wave impedance. First, we acquire the real and imaginary parts Z_r' and Z_r'' of the time-domain wave impedance, by truncating the frequency range from f_A to f_B to include the $\lambda/2$ resonance (see Fig. 2) and by performing the inverse discrete Fourier transform (DFT) (for example, see [22]) for the frequency responses of the real and

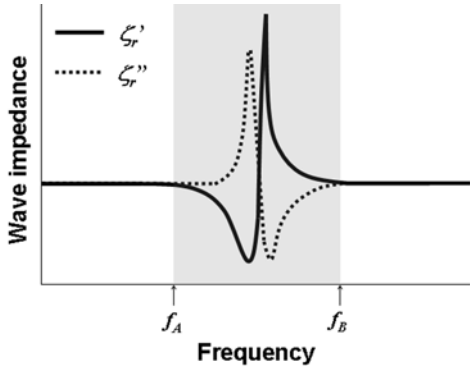

Figure 2. Conceptual drawing of the wave impedance frequency response for a low-loss material measured with the T/R method around a $\lambda/2$ frequency.

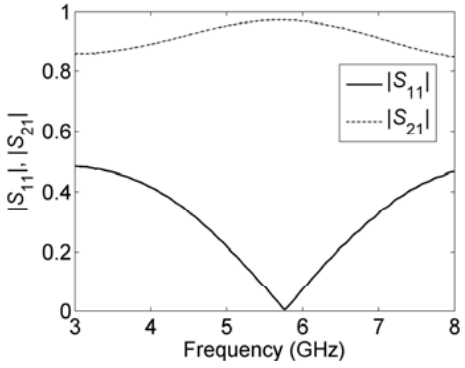

Figure 3. S-parameters measured for the nylon sample.

imaginary parts ς_r' and ς_r'', individually, such as

$$Z'_{r,p} = \sum_{k=0}^{N-1} \varsigma'_{r,k} \cdot \exp\left(\frac{j2\pi kp}{N}\right), \tag{12}$$

$$Z''_{r,p} = \sum_{k=0}^{N-1} \varsigma''_{r,k} \cdot \exp\left(\frac{j2\pi kp}{N}\right), \tag{13}$$

where p is the index for the time-domain data $p = 0, 1, 2, \ldots, N$, k is the index for the frequency-domain data $k = 0, 1, 2, \ldots, N$, and N is the number of the data points from f_A through f_B.

Consecutively, we apply windowing to Z'_r and Z''_r so that we can have zero-time components of Z'_r and Z''_r — unless we have only the zero-time components, the resultant frequency-domain wave impedance ς_r' and ς_r'' after windowing will still turn out to be oscillatory and resonant. The real and imaginary parts of the modified time-domain wave impedance are expressed as

$$Z'_{r,p(\text{windowed})} = w'_p \cdot Z'_{r,p}, \tag{14}$$

$$Z''_{r,p(\text{windowed})} = w''_p \cdot Z''_{r,p}, \tag{15}$$

where w'_p and w''_p are the window functions respectively for the real and imaginary parts of the wave impedance that permit *almost* only the zero-time components of the wave impedance:

$$w'_p,\, w''_p = \begin{cases} 1, & \text{for} \quad p = 0, 1, \ldots \text{ (small integer)} \\ 0, & \text{otherwise.} \end{cases} \tag{16}$$

Notice here that w'_p and w''_p are identical to a low-pass filter in the frequency domain that passes *almost* DC components. In general, $w'_p = 1$ and $w''_p = 1$ for $p = 0$ give reasonable results. However, if the measurement frequency range is very broad and the step size in the time domain after the inverse DFT is considerably small, $w'_p = 1$ and $w''_p = 1$ for $p = 0, 1, \ldots$ (p is a small integer) may be chosen, as long as the wave impedance $\varsigma'_{r(\text{smoothed})}$ and $\varsigma''_{r(\text{smoothed})}$ obtained with Eqs. (17) and (18) are sufficiently smooth. Note also that since oscillations in ς_r' and ς_r'' are not necessarily the same, w'_p and w''_p do not always need to be the identical window functions, and the window widths p for each w'_p, $w''_p = 1$ may be optimally chosen. In the final stage, we do the forward DFT (see [22]) to get frequency responses of the smoothed ς_r' and ς_r'':

$$\varsigma'_{r,k(\text{smoothed})} = \sum_{p=0}^{N-1} Z'_{r,p(\text{windowed})} \cdot \exp\left(-\frac{j2\pi kp}{N}\right), \tag{17}$$

$$\varsigma''_{r,k(\text{smoothed})} = \sum_{p=0}^{N-1} Z''_{r,p(\text{windowed})} \cdot \exp\left(-\frac{j2\pi kp}{N}\right), \tag{18}$$

The function of the windowing above is, in effect, an averaging of the resonant oscillatory wave impedance shown in Fig. 2. In practice, there are commercial numerical software packages available that facilitate prompt implementation of the inverse and forward DFTs in Eqs. (12), (13), (17), and (18) with built-in commands.

The acquisition of smoothed ε_r and μ_r can easily follow in conjunction with $\varepsilon_r = n/\varsigma_{r(\text{smoothed})}$ and $\mu_r = n \cdot \varsigma_{r(\text{smoothed})}$ where n is the refractive index obtained with Eq. (8).

3. RESULTS AND DISCUSSION

3.1. Measurement Results

For experimental validation of the method outlined in Section 2, we placed a test sample into an APC-7 coaxial sample fixture whose inner and outer radii are respectively $a = 1.52\,\text{mm}$ and $b = 3.50\,\text{mm}$,

and conducted S-parameter measurements for the loaded sample fixture with an HP 8510C VNA[†]. To perform these S-parameter measurements, we calibrated ports 1 and 2 at the ends of APC-7 cables attached to this VNA with the short-open-load-thru (SOLT) technique, before inserting the loaded sample fixture in between.

As the first validation study, we measured a sample of nylon that has a low-loss dielectric characteristic ($\varepsilon_r \cong 3$ and $\mu_r = 1$). The sample length is $L = 15.10$ mm. Fig. 3 shows S-parameter data measured for the nylon sample as a function of measurement frequency. It is seen from Fig. 3 that S_{11} and S_{21} become very small and large ($|S_{11}| \cong 0.005$ and $|S_{21}| \cong 0.974$) at 5.76 GHz where the sample length is found to be approximately a wavelength, $L \cong \lambda$.

Figures 4(a) and (b) give the plots of the refractive index n and wave impedance ς_r extracted from the S-parameters in Fig. 3 with the conventional T/R method, i.e., Eqs. (5)–(9). These plots show that frequency responses of extracted n' and n'' of nylon are very smooth over the entire frequency range, whereas in contrast, ς_r' and ς_r'' exhibit a very evident peak, as has been pointed out in Subsection 2.2.

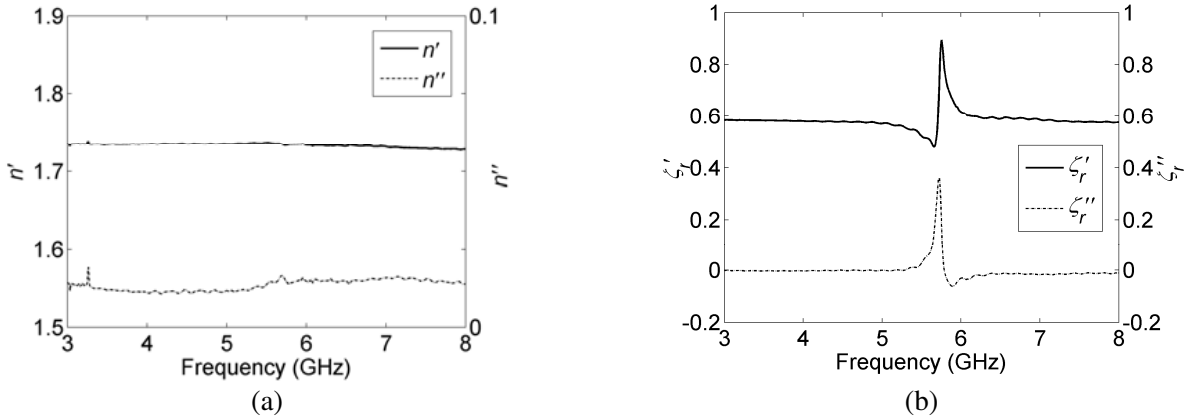

Figure 4. Refractive index and wave impedance extracted for the nylon with the T/R method. (a) n and (b) ς_r.

We now apply the time-domain smoothing outlined in Subsection 2.3 to the wave impedance in Fig. 4(b). We truncate the frequency range from $f_A = 4.87$ GHz through $f_B = 6.74$ GHz ($N = 301$) to perform the inverse DFT, since ς_r' and ς_r'' seem to be resonant in that frequency range. Figs. 5(a)–(d) present the real and imaginary parts of the time-domain wave impedance, Z_r' and Z_r'', before/after windowing. Only the magnitudes are shown in those plots and those values are normalized by the maximum values of the non-windowed one, e.g., $|Z'_{r(\text{non-windowed})}| / \max(|Z'_{r(\text{non-windowed})}|)$, $|Z'_{r(\text{windowed})}| / \max(|Z'_{r(\text{non-windowed})}|)$, etc. We confirm in Figs. 5(b) and (d) that only the zero-time components remain and all the other components are cut off by the windowing.

Figure 6(a) shows the smoothed and non-smoothed ς_r' and ς_r'' (the non-smoothed ones replicate those in Fig. 4(b)) as a function of frequency, which are obtained by the forward DFT applied to the time-domain wave impedance Z_r' and Z_r'', as plotted in Fig. 5. In Fig. 6(a), we see that both of the smoothed ς_r' and ς_r'' come out to be appropriately flat over the entire frequency range, with the smoothed $\varsigma_r' = 0.59$ and $\varsigma_r'' = 0.008$, while the non-smoothed ς_r' and ς_r'' have a maximum peak at 5.74 GHz. Figs. 6(b) and (c) give a comparison of the smoothed and non-smoothed permittivity and permeability calculated from Eqs. (10) and (11) with the help of the refractive index in Fig. 4(a) and the wave impedance in Fig. 6(a). The smoothed ε_r', ε_r'', ε_r', and μ_r'' can be validated to be adequately clean compared to the non-smoothed ones. The data in [11] are given in Fig. 6, and we can see that the present approach more accurately follows the conventional results outside the resonance, and provides a good interpolation to the material parameters, whereas the approximate results seem to slightly deviate from the smooth values of the conventional results outside the resonance. Further, from Fig. 6, we can

[†] Reference to specific hardware in this article is provided for informational purposes only and constitutes no endorsement by the National Institute of Standards and Technology.

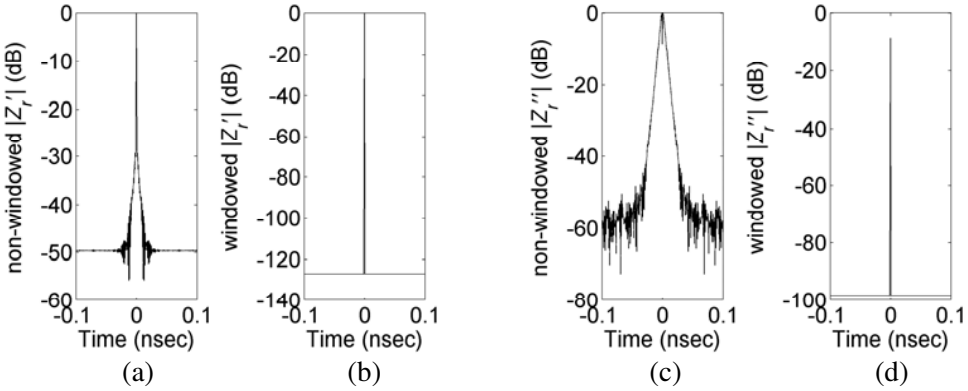

Figure 5. Real and imaginary parts of the time-domain wave impedance of the nylon sample before/after windowing. (a) Non-windowed $|Z'_r|$, (b) windowed $|Z'_r|$, (c) non-windowed $|Z''_r|$, and (d) windowed $|Z''_r|$.

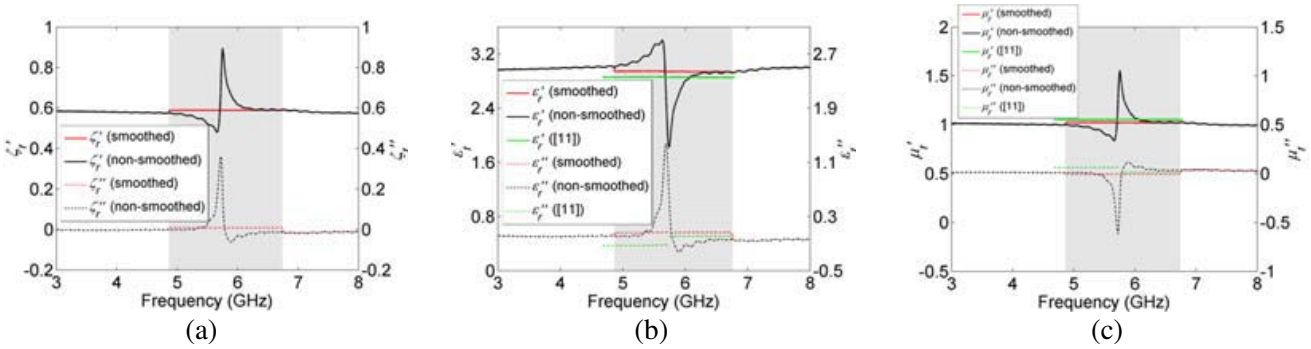

Figure 6. (a) Wave impedance ς_r, (b) permittivity ε_r, and (c) permeability μ_r computed before/after smoothing for the nylon sample along with the data in [11]. The gray regions in the graphs indicate the frequency range f_A–f_B truncated to apply the time-domain smoothing.

read the smoothed permittivity and permeability around the resonance to be $\varepsilon'_r = 2.94$, $\varepsilon''_r = 0.07$, $\mu'_r = 1.02$, and $\mu''_r = -0.005$ at 5.74 GHz. Those values are confirmed to successfully eliminate the artifacts that arise in the conventional T/R method and to accurately be almost flat as the values outside the resonance obtained with the T/R method, $\varepsilon_r \cong 3$ and $\mu_r \cong 1$.

For the second validation case, we measured a lithium ferrite sample that is a low-loss magnetic material with $\mu_r \neq 1$ unlike the nylon case. Many magnetic materials are known to generally possess strong dispersive characteristics in their permittivity and permeability.

S-parameters measured for the lithium ferrite sample with the APC-7 fixture are shown in Fig. 7. The length of the lithium ferrite sample is $L = 25.54$ mm, and we see in Fig. 7 that there are two evident resonances present near 4.2 GHz and 5.5 GHz, each of which corresponds to the frequencies where the sample becomes nearly $L \cong \lambda$ and $L \cong 1.5\lambda$, respectively.

The material parameters of the lithium ferrite are computed in the same manner as done for the nylon measurement. The smoothed and non-smoothed permittivity and permeability obtained for the lithium ferrite sample are given in Fig. 8, as well as the data in [11]. In order to smooth out those resonances, we first truncate the frequency ranges for f_A–f_B, at 4.0 GHz–4.595 GHz ($N = 121$) and at 5.195 GHz–5.795 GHz ($N = 121$), to individually include each of those resonances. After getting the inverse DFT done, one at a time, we apply windowing to each one, and we apply the forward DFT to acquire the frequency responses in each of the truncated frequency ranges again.

Figure 8 shows that the real and imaginary parts of both the smoothed ε_r and μ_r are sufficiently clean whereas those of the non-smoothed ones yield very sharp resonant peaks. As has been seen in

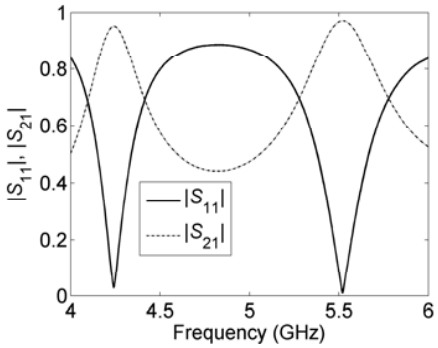

Figure 7. S-parameters measured for the lithium ferrite sample.

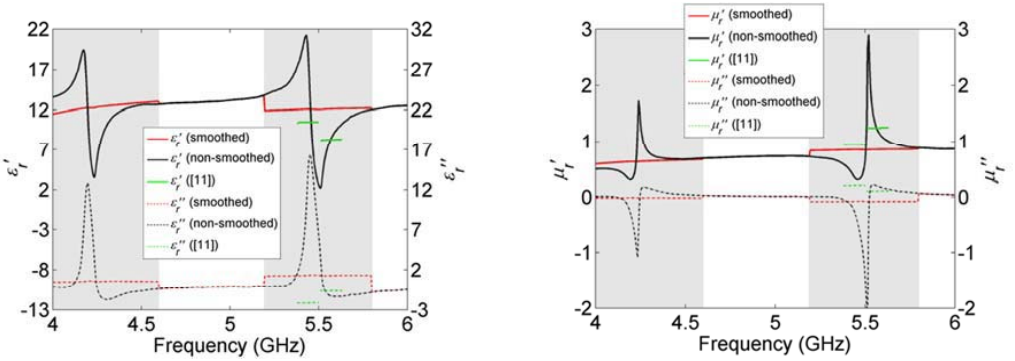

Figure 8. (a) Permittivity ε_r and (b) permeability μ_r computed before/after smoothing for the lithium ferrite along with the data in [11]. The gray regions in the graphs indicate the frequency ranges f_A–f_B truncated to apply the time-domain smoothing.

the nylon measurement case, the smoothed results appear to be more accurate than the results in [11]. We can also see that Figs. 8(a) and (b) show that the present approach, based on the time-domain smoothing technique, gives $\varepsilon_r = 12.28 - j0.58$ and $\mu_r = 0.63 + j0.01$ at 4.2 GHz and $\varepsilon_r = 12.07 - j1.31$ and $\mu_r = 0.84 + j0.08$ at 5.5 GHz.

3.2. Uncertainties

The rigorous evaluation of analytical uncertainties in the smoothed permittivity and permeability obtained with the method described in Subsection 2.3 is not straightforward. Here, the uncertainty analysis for only the 'non-smoothed' results with the conventional T/R method, i.e., Eqs. (5)–(9), in place of those of the smoothed ones, is presented — we will see, in the following, that the uncertainties for the non-smoothed results become very large and nearly maximum at the $\lambda/2$ resonance frequencies, and at the present stage, we speculate that the uncertainties for the 'smoothed' results would be smaller than those for the non-smoothed ones. Further, in order to calculate the analytical uncertainties, we assume that the sources of the uncertainties are systematic errors of magnitudes and phases of the measured S-parameters and the uncertainty in the sample length. For example, a total, differential uncertainty of the real part ε'_r of the non-smoothed permittivity is [8, 9],

$$\Delta\varepsilon'_r = \sqrt{\left(\frac{\partial\varepsilon'_r}{\partial|S_\alpha|}\Delta|S_\alpha|\right)^2 + \left(\frac{\partial\varepsilon'_r}{\partial\theta_\alpha}\Delta\theta_\alpha\right)^2 + \left(\frac{\partial\varepsilon'_r}{\partial L}\Delta L\right)^2}, \tag{19}$$

where $\alpha = 11$ or 21, $\Delta|S_\alpha|$ is the uncertainty in the magnitude of the S-parameter, $\Delta\theta_\alpha$ is the uncertainty in the phase of the S-parameter, and ΔL is the uncertainty in the sample length. Eq. (19) excludes the uncertainties that arise from errors in the sample fixture dimensional variations, the location of the

reference planes, etc., because it was reported that these uncertainties are generally smaller than those due to systematic measurement errors introduced by VNAs [23]. Further, Eq. (19) is also applicable to estimate the total uncertainties for $\Delta\varepsilon_r''$, $\Delta\mu_r'$, and $\Delta\mu_r''$, replacing $\partial\varepsilon_r'$, respectively, by $\partial\varepsilon_r''$, $\partial\mu_r'$, and $\partial\mu_r''$.

The expanded uncertainty U is defined as $U = ku_c$, where k is the coverage factor, and u_c is the combined standard uncertainty ($\Delta\varepsilon_r'$, $\Delta\varepsilon_r''$, $\Delta\mu_r'$, or $\Delta\mu_r''$ in this paper). If, for example, the normal distribution applies to u_c and $k = 2$, then the expanded uncertainty U gives an interval with a level of confidence of approximately 95% [24].

Figure 9 displays the expanded uncertainties U in the non-smoothed ε_r and μ_r of the nylon sample with the coverage factor $k = 2$. In general, the uncertainties should be properly represented as $+/-U$ rather than as the absolute values. For plotting Fig. 9, we use $\Delta|S_{11}| = \Delta|S_{21}| = 0.001$, $\Delta\theta_{11} = \Delta\theta_{21} = 0.02$ deg, and $\Delta L = 5\,\mu$m as measurement bounds. We observe in the plots in Fig. 9 that the expanded total uncertainties in the real and imaginary parts of the permittivity and permeability from Eqs. (5)–(9) attain their maximum values around 5.73 GHz near the frequency where we have seen the peaks of $|S_{11}|$ and $|S_{21}|$ in Fig. 3. This may be another perspective in addition to the discussion in Subsection 2.2 about what causes a resonant artifact at the $\lambda/2$ frequency.

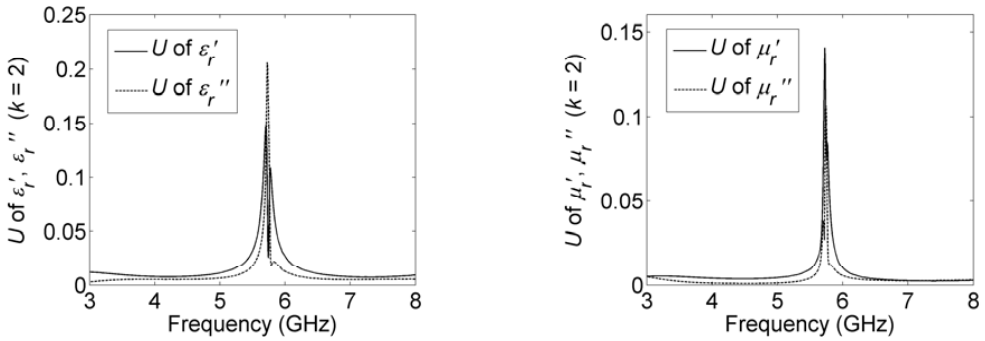

Figure 9. Expanded uncertainties in the non-smoothed permittivity and permeability of the nylon sample with the coverage factor $k = 2$.

In addition, we calculate the total uncertainties for the lithium ferrite sample with the same measurement bounds as for the nylon sample. Our calculation finds that the real and imaginary parts of the non-smoothed permittivity have maximal expanded uncertainties with $k = 2$, i.e., $+/-0.11$ and $+/-0.17$ at 4.2 GHz, and $+/-0.43$ and $+/-0.28$ at 5.5 GHz — these are near the frequencies where we have seen the resonances as in Fig. 7. The calculation provides large expanded uncertainties ($k = 2$) in the real and imaginary parts of the permeability at the same frequencies as for the permittivity — respectively, $+/-0.07$ and $+/-0.05$ at 4.2 GHz, and $+/-0.20$ and $+/-0.52$ at 5.5 GHz.

At present, we plan to perform a full uncertainty analysis for smoothed results for the present approach. The uncertainties for the smoothed results will be not only a function of the measured quantities, but also depend on how we choose f_A–f_B, the window functions, etc. To that end, we will need to accumulate measurement data by repeating measurements under the same measurement conditions, and statistically estimate the uncertainties rather than analytically compute them.

4. CONCLUSION

Employing the time-domain smoothing, we have developed a new approach for simultaneously determining complex permittivity and permeability that removes artifacts coming about at the $\lambda/2$ frequencies when measuring low-loss materials with the conventional T/R method. This present approach has been shown to generate sufficiently smooth permittivity and permeability of low-loss, moderately dispersive materials around the $\lambda/2$ resonances while the approximate parameters from our

previous approach [11] somehow deviated from reasonable results obtained with the conventional T/R method outside these resonances.

To derive the present approach, firstly, assuming that the refractive index n obtained with the conventional T/R method is adequately smooth at all frequencies, we have inversely discrete-Fourier transformed an f_A–f_B truncated frequency response of the wave impedance into the time domain. We have then applied windowing that allows for the zero-time components of the wave impedance and subsequently have conducted the forward DFT to recover the smoothed wave impedance $\varsigma_{r(\text{smoothed})}$ as a function of frequency. We calculated the complex permittivity and permeability in a way that $\varepsilon_r = n/\varsigma_{r(\text{smoothed})}$ and $\mu_r = n \cdot \varsigma_{r(\text{smoothed})}$.

We have validated the present approach by measuring two test materials, nylon and lithium ferrite. Our present approach has successfully yielded sufficiently flat permittivity and permeability of the nylon sample around the $\lambda/2$ resonance, and has shown to eliminate the resonant artifacts and provide very good interpolation that smoothly connects outside-resonance results from the conventional T/R method, $\varepsilon_r \cong 3$ and $\mu_r \cong 1$. The present approach has also extracted the permittivity and permeability of the lithium ferrite sample, showing reasonably smooth responses over the resonant frequency ranges. In both experimental validation cases, comparisons to the data in [11] have been given, and we have observed that the present approach generates more accurate ε_r and μ_r than does the technique in [11].

We should reiterate that the present approach has been derived to accurately measure low-loss materials removing $\lambda/2$ resonant artifacts and that any special treatment as the present or approximate technique would not be necessary for measurements on materials lossy enough to ensure sufficient stability of Eq. (9). Note also that accuracy of results with the present approach would depend on how we choose f_A–f_B and the window function for smoothing. At present, we choose the frequencies f_A and f_B so that that frequency range fully includes the resonance and the material parameters interpolate smooth values below/above the resonant frequencies. We plan to investigate the reasonable bounds of the material parameters determined with the conventional T/R method that enables us to select physically justifiable f_A and f_B where the extracted parameters start deviating from the real ones. Moreover, we will conduct a full uncertainty analysis for smoothed data that accounts for errors due to selection of f_A–f_B, the window functions, etc.

ACKNOWLEDGMENT

The authors thank Michael D. Janezic of the National Institute of Standards and Technology (NIST) in Boulder, Colorado, USA, for providing some S-parameter measurement data. The authors thank James Baker-Jarvis for very fruitful discussions on this work.

REFERENCES

1. Von Hippel, A. R., *Dielectric Materials and Application*, MIT Press, MA, 1961.
2. Chen, L. F., C. K. Ong, C. P. Neo, V. V. Varadan, and V. K. Varadan, *Microwave Electronics: Measurement and Materials Characterization*, Wiley, NJ, 2004.
3. Baker-Jarvis, J., M. D. Janezic, B. F. Riddle. R. T. Johnk, P. Kabos, C. L. Holloway, R. G. Geyer, and C. A. Grosvenor, "Measuring the permittivity and permeability of lossy materials: Solids, liquids, metals, building materials, and negative-index materials," National Institute of Standards and Technology Technical Note 1536, 2005.
4. Baker-Jarvis, J., M. D. Janezic, and D. C. De Groot, "High-frequency dielectric measurements," *IEEE Instrumentation and Measurement Magazine*, Vol. 13, No. 2, 24–31, 2010.
5. Nicolson, A. M. and G. F. Ross, "Measurement of intrinsic properties of materials by time-domain techniques," *IEEE Trans. Instrum. Meas.*, Vol. 19, No. 4, 377–382, 1970.
6. Weir, W. B., "Automatic measurement of complex dielectric constant and permeability at microwave frequencies," *Proc. IEEE*, Vol. 62, No. 1, 33–36, 1974.
7. Ligthart, L. P., "Fast computational techniques for accurate permittivity determination using transmission line methods," *IEEE Trans. Microw. Theory Tech.*, Vol. 31, No. 3, 249–254, 1983.

8. Baker-Jarvis, J., E. J. Vanzura, and W. A. Kissick, "Improved technique for determining complex permittivity with the transmission/reflection method," *IEEE Trans. Microw. Theory Tech.*, Vol. 38, No. 8, 1096–1103, 1990.
9. Baker-Jarvis, J., M. D. Janezic, J. H. Grosvenor, Jr., and R. G. Geyer, "Transmission/reflection and short-circuit line method for measuring permittivity and permeability," National Institute of Standards and Technology Technical Note 1355-R, 1993.
10. Boughriet, A.-H., C. Legrand, and A. Chapton, "Noniterative stable transmission/reflection method for low-loss material complex permittivity determination," *IEEE Trans. Microw. Theory Tech.*, Vol. 45, No. 1, 52–57, 1997.
11. Kim, S. and J. Baker-Jarvis, "An approximate approach to determining the permittivity and permeability near $\lambda/2$ resonances in transmission/reflection measurements," *Progress In Electromagnetics Research B*, Vol. 58, 95–109, 2014.
12. Chalapat, K., K. Sarvala, J. Li, and G. S. Paraoanu, "Wideband reference-plane invariant method for measuring electromagnetic parameters of materials," *IEEE Trans. Microw. Theory Tech.*, Vol. 57, No. 9, 2257–2267, 2009.
13. Qi, J., H. Kettunen, H. Wallen, and A. Sihvola, "Compensation of Fabry-Pérot resonances in homogenization of dielectric composites," *IEEE Antennas Wireless Propag. Lett.*, Vol. 9, 1057–1060, 2010.
14. Liu, X.-X., D. A. Powell, and A. Alù, "Correcting the Fabry-Pérot artifacts in metamaterial retrieval procedures," *Phys. Rev. B*, Vol. 84, 235106, 2011.
15. Smith, D. R. and S. Schultz, "Determination of effective permittivity and permeability of metamaterials from reflection and transmission coefficients," *Phys. Rev. B*, Vol. 65, 195104, 2002.
16. Chen, X., T. M. Grzegorczyk, B.-I. Wu, J. Pacheco, Jr., and J. A. Kong, "Robust method to retrieve the constitutive effective parameters of metamaterials," *Phys. Rev. E*, Vol. 70, 016608, 2004.
17. Kim, S., E. F. Kuester, C. L. Holloway, A. D. Aaron, and J. Baker-Jarvis, "Boundary effects on the determination of metamaterial parameters from normal incidence reflection and transmission measurements," *IEEE Trans. Antennas Propag.*, Vol. 59, No. 6, 2226–2240, 2011.
18. Kim, S., E. F. Kuester, C. L. Holloway, A. D. Scher, and J. R. Baker-Jarvis, "Effective material property extraction of a metamaterial by taking boundary effects into account at TE/TM polarized incidence," *Progress In Electromagnetics Research B*, Vol. 36, 1–33, 2012.
19. Lefrançois, S., D. Pasquet, and G. Mazé-Merceur, "A new model for microwave characterization of composite materials in guided-wave medium," *IEEE Trans. Microw. Theory Tech.*, Vol. 44, No. 9, 1557–1562, 1996.
20. Starostenko, S. N. and A. P. Vinogradov, "The reflectivity discrepancy method for the determination of the permittivity and permeability of complex materials," *IEEE Trans. Instrum. Meas.*, Vol. 51, No. 1, 125–132, 2002.
21. Barroso, J. J. and A. L. de Paula, "Retrieval of permittivity and permeability of homogeneous materials from scattering parameters," *Journal of Electromagnetic Waves and Applications*, Vol. 24, Nos. 11–12, 1563–1574, 2010.
22. James, J. F., *A Student's Guide to Fourier Transforms: With Applications in Physics and Engineering*, 3rd Edition, Cambridge University Press, NY, 2011.
23. Hill, D. A., "Reflection coefficient of a waveguide with slightly uneven walls," *IEEE Trans. Microw. Theory Tech.*, Vol. 37, No. 1, 244–252, 1989.
24. Taylor, B. N. and C. E. Kuyatt, "Guidelines for evaluating and expressing the uncertainty of NIST measurement results," National Institute of Standards and Technology Technical Note 1297, 1994.